HHS Public Access

Author manuscript

Nat Commun. Author manuscript; available in PMC 2014 September 04.

Published in final edited form as:

Nat Commun. ; 5: 3416. doi:10.1038/ncomms4416.

Mutations in Alström Protein Impair Terminal Differentiation of Cardiomyocytes

Lincoln T. Shenje[1,*], **Peter Andersen**[1,*], **Marc K. Halushka**[2], **Cecillia Lui**[1], **Laviel Fernandez**[1], **Gayle B. Collin**[3], **Nuria Amat-Alarcon**[1], **Wendy Meschino**[4], **Ernest Cutz**[5], **Kenneth Chang**[5,6], **Raluca Yonescu**[2,7], **Denise A. S. Batista**[2,7], **Yan Chen**[1], **Stephen Chelko**[1], **Jane E. Crosson**[8], **Janet Scheel**[8], **Luca Vricella**[9], **Brian D. Craig**[7], **Beth A. Marosy**[7], **David W. Mohr**[7,10], **Kurt N. Hetrick**[7], **Jane M. Romm**[7], **Alan F. Scott**[7,10], **David Valle**[7], **Jürgen K. Naggert**[3], **Chulan Kwon**[1], **Kimberly F. Doheny**[7], and **Daniel P. Judge**[1]

[1]Division of Cardiology, Department of Medicine, Johns Hopkins University School of Medicine, Baltimore, MD, 21287 USA

[2]Department of Pathology, Johns Hopkins University School of Medicine, Baltimore, MD, 21287 USA

[3]The Jackson Laboratory, Bar Harbor, ME, 04609 USA

[4]North York General Hospital, Toronto, ON, M2K 1E1 Canada

[5]Division of Pathology, Department of Paediatric Laboratory Medicine, The Hospital for Sick Children, Toronto, ON, M5G 1X8 Canada

[6]KK Women's and Children's Hospital and Duke-NUS Graduate Medical School, Singapore 229899

[7]McKusick-Nathans Institute of Genetic Medicine, Johns Hopkins University School of Medicine, Baltimore, MD, 21287 USA

[8]Division of Cardiology, Department of Pediatrics, Johns Hopkins University School of Medicine, Baltimore, MD, 21287 USA

Corresponding author: Daniel P. Judge, MD, Center for Inherited Heart Disease, Johns Hopkins University School of Medicine, 720 Rutland Avenue, Ross #1049, Baltimore, MD 21205 USA, Phone +001 410-614-3085, djudge@jhmi.edu.
*These 2 authors contributed equally to the work.

Author Contributions D.P.J. managed and supervised the project. L.T.S., P.A., and M.K.H. performed the histological analyses. P.A., L.T.S., L.F., N.A.A., Y.C., and S.C. performed the cellular studies. C.L., W.M., E.C, and K.C. characterized the Canadian samples. G.B.C and J.K.N developed, characterized, and provided the *Alms1*-mutant mice. R.Y. and D.A.S.B. performed the ploidy analyses. J.E.C, J.S., and L.V. identified, characterized, and referred the proband and her sibling. B.D.C, B.A.M., D.W.M, K.N.H., J.M.R., A.F.S, D.V., and K.F.D. performed the exome sequencing and bioinformatics analysis. L.T.S., P.A., C.K., and D.P.J. designed the experiments, interpreted the data, wrote and revised the manuscript.

Conflict of Interests The authors declare no competing financial interests.

Accession Codes:
Whole exome sequence data for the proband has been deposited in the GenBank dbGaP (database of Genotypes and Phenotypes) database under the accession code phs000711.v1.p1. Sequence data for *ALMS1* from additional patients have been deposited in the GenBank nucleotide core database under the accession codes AB905563 to AB905565.

[9]Division of Cardiothoracic Surgery, Department of Surgery, Johns Hopkins University School of Medicine, Baltimore, MD, 21287 USA

[10]High Throughput Sequencing Facility, Genetic Resources Core Facility, McKusick-Nathans Institute of Genetic Medicine, Johns Hopkins University School of Medicine, Baltimore, MD, 21287 USA

Abstract

Cardiomyocyte cell division and replication in mammals proceed through embryonic development and abruptly decline soon after birth. The process governing cardiomyocyte cell cycle arrest is poorly understood. Here we carry out whole exome sequencing in an infant with evidence of persistent postnatal cardiomyocyte replication to determine the genetic risk factors. We identify compound heterozygous *ALMS1* mutations in the proband, and confirm their presence in her affected sibling, one copy inherited from each heterozygous parent. Next, we recognise homozygous or compound heterozygous truncating mutations in *ALMS1* in four other children with high levels of postnatal cardiomyocyte proliferation. *Alms1* mRNA knockdown increases multiple markers of proliferation in cardiomyocytes, the percentage of cardiomyocytes in G2/M phases, and the number of cardiomyocytes by 10% in cultured cells. Homozygous *Alms1*-mutant mice have increased cardiomyocyte proliferation at two weeks postnatal compared to wild-type littermates. We conclude that deficiency of Alström protein impairs postnatal cardiomyocyte cell cycle arrest.

Mammalian cardiac development requires continuous proliferation of cardiomyocytes throughout gestation[1,2]. During the perinatal period, cardiomyocyte proliferation rapidly declines, and the majority of cardiomyocytes undergo cell cycle arrest with terminal differentiation[3,4]. Postnatal arrest of the cardiomyocyte cell cycle is a key event for maturation of the mammalian heart, but this process is poorly understood[3]. A recent report highlights the role of the homeodomain transcription factor, Meis1, as a critical regulator of postnatal cardiomyocyte cell cycle arrest, though this process remains incompletely understood[5].

Unusual human phenotypes sometimes offer the opportunity to understand normal development or disease pathogenesis, if the cause can be determined. Mitogenic cardiomyopathy is a rare form of pediatric cardiomyopathy characterized by persistent markers of mitotic activity in cardiomyocytes[6]. Among five previously reported infants with this condition, there were two pairs of siblings, one of whom had parental consanguinity supporting a recessive genetic disorder. Although transgenic models of postnatal cardiomyocyte replication have been developed, no naturally inherited conditions have previously been characterized in humans that are associated with delayed postnatal cardiomyocyte cell cycle arrest[7,8]. Recognition and characterization of such a disorder has the potential to identify important regulators of the transition of cardiomyocytes from active proliferation to terminal differentiation.

Here we identify *ALMS1* mutations in 2 siblings and 4 previously reported infants with “mitogenic cardiomyopathy.” We show that siRNA-induced knockdown of murine *Alms1* increases cell cycle progression in cultured neonatal murine cardiomyocytes, and *Alms1*

knockdown also increases the number of induced cardiomyocytes in counting experiments. Mice with targeted mutation of *Alms1* have delayed exit from active cell cycle progression, further supporting an important role for ALMS1 in regulating postnatal cardiomyocyte cell cycle arrest.

Results

Evaluation of the proband and her sibling

We identified two infant siblings with neonatal heart failure, both of whom required cardiac transplantation. The proband was normal at birth, and she had no other manifestations of Alström syndrome prior to transplantation, which was performed at three months of age. The proband's only sibling underwent cardiac transplantation at age five months for similar cardiac dysfunction. Intracranial bleeding complicated her post-operative course, and she died one month later. Cardiac evaluations of both parents were normal. We visualized mitotic cardiomyocytes with antibodies against phosphorylated histone H3 (PH3, a marker for M-phase[9]) and cardiac troponin T (cTnT) (Figure 1a, b, c, and d) and as well as wheat germ agglutinin (WGA) to distinguish cell boundaries (Figure 2). Using an unbiased double-blinded approach for quantification of proliferating myocytes, we quantified PH3-positive cardiomyocytes in multiple fields from the proband and three age-matched controls with heart failure. The amount of PH3-positive cardiomyocytes was higher in the proband than in the controls (114.3 ± 31.3 per mm^2 [N=4] vs. 0.28 ± 0.07 per mm^2 [N=12], Student's *t*-test, mean ± S.E.M., respectively). To validate the high number of proliferating cardiomyocytes in the proband, we stained with antibodies against phospho-aurora kinases (PAK) A, B, and C. PAK A/B/C are important regulators of karyokinesis and cytokinesis, and localization of phospho-aurora kinase B to the cleavage furrow is required for establishing cytokinesis[10]. Aurora kinases are essential for formation of the mitotic spindle, separation of centrosomes and assembly of the cleavage furrow during pro-, meta-, ana, and telophase of mitosis[10–12]. Immunostaining for PAK confirmed an increase in the number of positively stained cardiomyocytes in multiple fields from the proband compared to the age-matched controls with heart failure (12.2 ± 2.6 per mm^2 [N=4] vs. $\leq 0.02 \pm 0.01$ per mm^2 [N=12], Student's *t*-test, mean ± S.E.M., respectively) (Figure 1e, f).

The proband underwent clinical genetic testing to determine the cause of her cardiomyopathy with a resequencing array[13]. Analysis of *MYH7, MYBPC3, TNNT2, TNNI3, TPM1, ACTC, LMNA, SGCD, EMD, DES, LDB3, ACTN2, CSRP3, TCAP, VCL, TAZ, PLN, ABCC9*, and *CTF1* showed no apparent cause for cardiomyopathy. Next, we performed whole exome sequencing using DNA obtained from the affected proband and both of her parents. With the presumption of a recessive disorder, we focused on missense, nonsense, or splice site variants that were likely to be compound heterozygote mutations in the affected offspring, since the ethnicity of the parents was geographically distant (northern European and Southeast Asian). Variants present in dbSNP131 or the 1000 genomes pilot April 2010 dataset were filtered out. After this level of filtering, six genes with compound missense variants and one gene with compound heterozygote frameshift insertion/deletion remained (Table 1). The 1000 genomes November 2010 data were subsequently available, and three of these genes with previously novel compound heterozygous missense variants were

filtered. Sanger sequencing confirmed novel DNA variants in each of the remaining four genes. The absence of one or both variants in the affected sibling led to filtering of two additional genes. *FERMT1* had two novel missense alleles (p.Arg98Cys and p.Val519Leu) that were present in each of the affected individuals. These novel variants in *FERMT1* were prioritized lower than *ALMS1* because Arg98 is not highly conserved (Cys in *Danio rerio*), and because valine and leucine are both neutral nonpolar amino acids (Grantham score 32); both variants are present at low levels in the NHLBI Exome Variant Server. We identified and confirmed two heterozygous *ALMS1* mutations in the proband and her sibling, both of which result in frameshift and premature termination (c.1794_1801dup8 in exon 8 and c. 11116_11134del19 in exon 16). Mutations in *ALMS1* are known to cause Alström syndrome, a recessive systemic disorder[14]. The c.11116_11134del19 mutation was previously reported in a patient with Alström syndrome[15]. Each parent harbored one of the mutant *ALMS1* alleles. Alström syndrome (OMIM #203800) is a recessive ciliopathy caused by *ALMS1* mutations and characterized by childhood truncal obesity, insulin-resistant diabetes mellitus, sensorineural hearing loss, retinal degeneration, and systemic fibrosis affecting multiple organs (kidney, liver, lung, and heart)[16,17]. Cardiomyopathy manifests in approximately two-thirds of affected individuals, and it can precede all other manifestations, obscuring the diagnosis of Alström[18,19]. We hypothesized that the mutations in *ALMS1* caused the delayed terminal differentiation of cardiomyocytes.

ALMS1 mutations in similarly affected infants

To extend these findings, we sequenced *ALMS1* in four additional infants (two sibling pairs) with mitogenic cardiomyopathy, from whom DNA was available[6]. We identified homozygous or compound heterozygous mutations in each of them (Table 2). For all cellular and immunohistochemical quantifications, unpaired two-tailed Student's *t*-test, type II, was used for data analysis, and $P \leq 0.5$ was considered significant. Using the same double-blinded quantification method described above, we quantified PH3-positive cardiomyocytes in three affected individuals (one from each sib-pair) and compared to three age-matched controls with heart failure, and found it to be higher in the affected children (67.3 ± 8.6 per mm^2 compared to 0.28 + 0.07 per mm^2, respectively, N=3, mean ±S.E.M., $P<0.01$; Figure 1g). Accordingly, DNA content in dividing cardiomyocytes was 1.9-fold greater in PH3-positive myocytes than in non-dividing cells, confirming that PH3-positive myocytes are undergoing mitosis (Figure 3).

Cardiomyocytes can undergo DNA replication without completing the cell cycle. Polyploidization occurs during early postnatal development and in response to myocardial stress[4,20,21]. We considered the possibility that ALMS1-deficiency could result in increased polyploidy. We applied centromeric FISH probes to determine the ploidy status in these infants with mitogenic cardiomyopathy. The percentage of 4N cardiomyocytes was 31.1+7.2% among affected individuals (N=4) and 15.5+8.3% in the controls (N=12), Student's *t*-test, mean±S.E.M., P=0.26. Although we found cardiomyocytes that were polyploid (>4N), there was no difference between affected individuals (0.4%, N=4) and failing heart age matched controls (0.6%, N=2) (Figure 3). Taken together, these results indicate that ALMS1 deficiency in cardiomyocytes does not lead to increased polyploidy.

Alms1 knockdown increases cardiomyocyte cell cycling

To confirm that ALMS1 loss is sufficient for extending the postnatal proliferative window of cardiomyocytes, we treated cultured neonatal mouse cardiomyocytes with *Alms1* siRNA (Supplementary Fig. 1). After 48 hours, cells were stained with antibodies against Ki67 (a wide-ranging marker of proliferation) or Vybrant DyeCycle Ruby Stain (a marker of DNA content for determination of cell cycle; Invitrogen), together with cTnT, and analyzed by flow cytometry. In ALMS1-deficient cardiomyocytes, Ki67-positive cardiomyocytes were 2.5-fold higher compared to control (4.2% vs. 1.7% respectively; N=8, Student's *t*-test, $P<0.05$) (Supplementary Fig. 2). Likewise, we observed more cells in G2/M phases after *Alms1* knockdown compared to the control (13.3+1.8% vs. 9.6+1.3% mean ± S.E.M., N=4, respectively; Student's *t*-test, $P<0.05$) (Figure 4). We also analyzed Ki67 expression in cells stained with the fibroblast marker Thy-1[22] and found no significant difference between ALMS1-deficient cardiac fibroblasts compared to control (3.5±0.5% vs. 2.9±0.8% mean ± S.E.M., N=4, respectively; Student's *t*-test, $P=0.55$), indicating that the observed increase of cells in G2/M may be in cardiomyocytes. To determine whether the observed increase in G2/M was mediated by cardiomyocytes, we cultured neonatal mouse cardiomyocytes obtained from transgenic mice in which the αMHC promoter drives expression of green fluorescent protein (GFP), and thus only cardiomyocytes produce GFP[23]. After *Alms1* knockdown, the number of GFP-positive cells in phases G2/M was increased compared to the control (11.3±1.0% vs. 7.0±0.9% mean ± S.E.M., N=3, respectively, Student's *t*-test, $P<0.05$) (Figure 5a), indicating that ALMS1-deficiency leads to impaired cell cycle arrest in cardiomyocytes.

To confirm that ALMS1-deficient cardiomyocytes proliferate with impaired cell cycle arrest, we differentiated cardiomyocytes from mouse ESCs that carry a cardiomyocyte-specific promoter (*Ncx1*), which drives puromycin resistance, allowing efficient purification of cardiomyocytes (>98%)[24]. (Supplementary Fig. 3) By immunohistochemistry, we confirmed the presence of cardiomyocytes in pro-, meta-, ana- and telophase of mitosis after knockdown of *Alms1* (Figure 5b, c, d, e), demonstrating that these cardiomyocytes complete the cell cycle in vitro. In accordance with this observation, the amount PAK-positive cardiomyocytes was higher in ALMS1-deficient cardiomyocytes compared to control (0.41±0.09% vs. 0.15±0.03%; mean ± S.E.M., N=3, respectively, Student's *t*-test, $P<0.05$; Figure 5f).

To confirm that ALMS1 loss extends the proliferative window of cardiomyocytes, we treated puromycin-selected cardiomyocytes with *Alms1* siRNA or control siRNA. After 48 hours, we pulse-labeled cardiomyocytes with 5-ethynyl-2′-deoxyuridine (EdU) for 12h. We observed an increase in EdU-positive cardiomyocytes after *Alms1* knockdown compared to controls (13.6 ± 1.0% vs. 10.2 ± 0.6%, mean ± S.E.M., N=15, respectively, Student's *t*-test, $P<0.05$)(Figure 5g). During maturation, cardiomyocytes undergo karyokinesis (nuclear division) but not cytokinesis (cell division) and become terminally differentiated[25]. To exclude the possibility that the observed increase in EdU-positive uptake is due to karyokinesis and not cytokinesis, we counted cardiomyocytes 72 hours after siRNA treatment and found that the number of cardiomyocytes was higher after *Alms1* knockdown compared to control (51,915±1821/cm^2 vs. 46,696±1311/cm^2, mean ± S.E.M., N= 4,

respectively; Student's *t*-test, P<0.05) (Figure 5h). Taken together, these results confirm that ALMS1-deficiency increases cardiomyocyte proliferation in vitro.

Impaired cardiomyocyte cell cycle arrest in *Alms1*$^{Gt/Gt}$ mice

To investigate the role of ALMS1 in vivo, we utilized *Alms1*$^{Gt/Gt}$ mice with truncated *Alms1* mRNA and many characteristics of human Alström syndrome[26]. In mice, the maturation process from mono- to binucleate state occurs during postnatal day 5–10, resulting in 95–99% cardiomyocytes being binucleated and terminally differentiated at 10 days of age[21,25]. We therefore analyzed mouse hearts at 15.5 days of age for persistent cardiomyocyte proliferation. To do this, we treated 15-day old mice with a pulse-dose of EdU, and 12 hours later, their hearts were isolated and EdU uptake in cardiomyocytes was analyzed using the double-blinded quantification method described above. In the *Alms1*$^{Gt/Gt}$ mutant mice, more than 8% of cardiomyocytes were EdU-positive, compared to very low levels in the wild-type littermate controls (8.3 ± 0.91% vs. 0.3 ± 0.04%, mean ± S.E.M., N=4, respectively; Student's *t*-test, P<0.001, Figure 6a, b, and c). Accordingly, we also observed a higher number of PH3-positive cardiomyocytes in homozygous *Alms1*$^{Gt/Gt}$ mutant mice compared to their wild-type littermates (13.2 ± 2.6 per mm^2 compared to less than 1 per mm^2; mean ± S.E.M., N= 3, Student's *t*-test, P<0.01)(Figure 6d, e, and f). Additional staining demonstrated increased PAK-positive cardiomyocytes in the *Alms1*$^{Gt/Gt}$ mice compared to wild-type controls (1.36 ± 0.1 vs. 0.11 ± 0.1 per mm^2; mean ± S.E.M., N= 3, Student's *t*-test, respectively; P<0.001)(Figure 6g, h, and i). Importantly, we did not observe any difference in apoptosis (caspase3-positive or TUNEL-positive cells) between *Alms1*$^{Gt/Gt}$ mutant mice and their littermate controls (Supplementary Fig. 4, 5).

Phenotypic characterization of *Alms1*$^{Gt/Gt}$ at postnatal day 15.5 demonstrated that ALMS1-mutant mouse heart/body ratio was larger in *Alms1*$^{Gt/Gt}$ mice (N=7) compared to wild-type littermates (N=16) (7.2 ± 0.3 vs. 6.4 ± 0.2; mean ± S.E.M., Student's *t*-test, P<0.05; Figure 7). In addition, *Alms1*$^{Gt/Gt}$ cardiomyocytes were smaller compared to wild-type littermate controls (128.2 ± 10.6 vs. 176.1 ± 8.5 μM^2, mean ± S.E.M., N= 4, Student's *t*-test, P < 0.0.001) (Figure 7), implying that cardiomyocyte number is increased in *Alms1*$^{Gt/Gt}$ hearts. Together, these findings indicate that terminal differentiation is impaired in ALMS1-deficient cardiomyocytes and that ALMS1-deficient cardiomyocytes remain proliferative beyond the normal window of postnatal cardiomyocyte cell cycle arrest. *Alms1* levels in dividing cardiomyocytes obtained from proliferative mouse hearts (embryonic day 15.5) are relatively low, compared to levels at the beginning of the maturation process (postnatal day 6) when cytokinesis rapidly declines, suggesting that ALMS1 may be transcriptionally regulated during perinatal development (Figure 8).

We considered whether our findings could be due to an increased number of cardiac stem cells. However we observed no difference in the number of c-kit+ or Sca-1+ cardiac stem cell markers in *Alms1*$^{Gt/Gt}$ compared to littermates (both markers <1 cell per 225 μM^2). As cardiac stem cells differentiate, they may lose c-kit or Sca-1 markers. Thus, we cannot exclude that the increase in proliferating cardiomyocytes may arise in part from resident cardiac stem cells.

Discussion

Our data show that ALMS1 is a key molecule for cell cycle regulation in perinatal cardiomyocytes. ALMS1 is a component of the non-motile primary cilium, a subcellular organelle that projects from most cell types. Its presence is temporally associated with cellular quiescence, with resorption during mitosis[27]. Induction of a longer cilium causes delay in G1/S transition, and ciliary disassembly increases S-phase[28,29]. Prior reports show that certain components of the primary cilium restrain canonical Wnt/β-catenin signaling, which plays an important role in cardiomyogenesis[30,31]. Deficiency of ALMS1 may activate Wnt/β-catenin signaling, thereby activating the transcription factor TCF/LEF (T-cell factor/lymphoid enhancer factor) and inducing transcription of genes that promote cell cycle proliferation[32,33].

Definitive proof of cardiomyocyte cytokinesis can be challenging. Proliferation markers, such as PH3, Ki67, and EdU, cannot discern karyokinesis from cytokinesis. Increased PAK staining in humans and mice with ALMS1 deficiency is consistent with increased cytokinesis, but it is insufficient. The increased density of cardiomyocytes in *Alms1*-mutant mice and the increased number of cardiomyocytes with cell counting studies after *Alms1* knockdown are further supportive of amplified cardiomyocyte cytokinesis. However, the evidence for cytokinesis, and therefore the completion of mitosis, is inconclusive and warrants further investigation.

Mitogenic cardiomyopathy is a very rare human phenotype, previously of unknown etiology. Our finding of homozygous or compound heterozygous mutations in *ALMS1* among all six affected infants from whom DNA was available suggests that this is the main cause. However, in each of these individuals, hearts were removed either at the time of transplantation due to end-stage heart failure or after death from heart failure[6]. Cardiomyopathy is found in approximately two-thirds of affected individuals, which suggests that other factors contribute to its development besides *ALMS1* mutations[18]. When cardiomyopathy develops in infancy, it can precede other manifestations, at times obscuring the diagnosis of Alström syndrome, as among these 6 infants and as previously reported[19]. The cardiac function of the ALMS1-mutant mice is normal[26]. However, our findings do not rule out an injury response that contributes to myocyte proliferation in the context of an *ALMS1* mutation.

ALMS1 localizes to the centrosome, which plays a pivotal role in regulation of the cell cycle[34,35]. At postnatal day 15 (1 week beyond the normal window of postnatal cardiomyocyte cell cycle arrest), ALMS1-deficient mice display persistent cardiomyocyte proliferation, indicating that ALMS1-deficient cardiomyocytes may have an impaired ability to undergo cell cycle arrest. A similar finding was previously reported for the transcription factor MEIS1, although no direct link between MEIS1 and ALMS1 is currently known[5]. Throughout mitosis, ALMS1 localizes to the centrosomal spindle poles, and during late mitosis, ALMS1 localizes to the contractile ring and the cleavage furrow[36]. ALMS1 retains the centrosome cohesion protein C-NAP1, an important regulator of centrosome organization during mitosis. Depletion of ALMS1 reduces centrosomal levels of C-NAP1 and increases centrosome splitting, a key event for chromosomal division during

anaphase[34]. In addition, ALMS1 interacts with several cytoskeleton-associated components that are necessary for the recycling of receptors to the plasma membrane, also referred to as endocytic trafficking[36]. During mitosis endocytic trafficking is repressed, as continued endocytosis may interfere with accurate chromosome segregation[37–39]. Interestingly, endocytic trafficking is significantly reduced in ALMS1-deficient cells[36]. Whether the impairment of terminal differentiation of cardiomyocyte proliferation is partly due to diminished endocytic trafficking remains unclear. Further investigation of this role of ALMS1 may identify novel and therapeutically important avenues to alter cardiomyocyte replication.

Methods

Exome sequencing

All human subjects (or their legal representative) signed informed consent, and the research was approved by the Johns Hopkins University Institutional Review Board. Genomic DNA was obtained from the proband's dermal fibroblasts and from blood from each of the parents by the Gentra Puregene Tissue/Blood Kit (Qiagen). Three μg of genomic DNA was sheared using the Covaris S-2 instrument (Covaris) using the recommended settings according to the Agilent protocol (SureSelect^{XT} Target enrichment System for Illumina Paired End and Multiplexed Sequencing Library v1.0) for a 150–200bp fragment size. Libraries were prepared for targeted enrichment using the SPRIworks Fragment Library System I (200–400bp size selection) according to Beckman-Coulter's protocol (version 2.0). Adapter ligated fragments were amplified according to the Agilent protocol for 6 cycles; 500ng of amplified library was used in a whole exome enrichment reaction with the SureSelect Human All Exon, 50 Mb product (Agilent WE). Samples were clustered one per flow cell lane using the Illumina cBot Paired End Cluster Generation Kit with v1 HiSeq flow cell (Illumina). Seventy-six bp paired-end sequencing was performed on the HiSeq2000 with TruSeq SBS v1 chemistry (Illumina).

Intensity analysis and base calling were performed through the Illumina Real Time Analysis (RTA) software (version 1.7.48.0). Average sequence yield for the samples was 9.2 Gb having a quality value of Q30 or greater. Basecall files were converted from a binary format (BCL) to flat file format (qseq.txt) using the Illumina BCL Converter software (version 1.7.1).

Basecall files were converted to fastq format, aligned with BWA[40] version 0.5.7 to the GRCh37 human genome reference. Duplicate molecules were flagged with Picard version 1.26. SNVs and indels were called using SAMtools[41] version 0.1.7. Only variant calls from the reference genome having a minimum depth of 10x were considered for downstream analysis. In addition, for SNVs, only those calls where the root mean square of their read mapping qualities (RMS) was greater than 20 were considered while for indels only those with an RMS greater than 15 were considered.

Samples were processed on the Illumina Infinium HumanOmniExpress beadchip (OE) to confirm family and gender relationships and provide sample identity confirmation against the sequencing data. The mean on bait coverage (regions covered by probes in the Agilent

WE) was greater than 77x for each sequencing experiment and greater than 92% of on bait bases had a depth greater than 10x. Overall concordance to genotypes for each sample was greater than 99.5%. Greater than 93% of the OE heterozygote genotypes for each sample within the baited regions were called as variants against reference in the sequencing experiments.

All remaining variants were annotated using the SeattleSeq Annotation Server build 6.03[42]. Variants present in dbSNP131 or the 1000 genomes pilot April 2010 dataset were filtered out. Only missense, nonsense or splice site compound heterozygotes present in the offspring where one allele each was inherited from the parents were considered. After this level of filtering, 6 compound missense heterozygotes and 1 compound heterozygote frameshift indel remained.

Statistical analyses

For all cellular and immunohistochemistry quantification, the unpaired two-tailed Student's *t*-test, type II, was used for data analyses. $P<0.05$ was considered significant.

Cell culture and analysis

Mouse neonatal cardiomyocytes were isolated from newborn mouse hearts on PD0.5. Hearts were minced and digested with collagenase type II and pancreatase myocyte digestion buffer. To enrich for cardiomyocytes, dissociated cells were pre-plated by the conventional pre-plating method[22,43]. Enriched cardiomyocytes were cultured in Dulbecco's Modified Eagle Medium (GIBCO) supplemented with 20% horse serum and 2 mM GlutaMAX (Invitrogen) in 5% CO2. Cardiac fibroblasts were identified by their expression of the cardiac fibroblast marker Thy-1[22,23]. Mouse embryonic stem cells (mESCs) carrying a puromycin resistance cassette driven by the cardiomyocyte-specific sodium-calcium exchanger 1 gene (*Ncx1*) promoter[44] were maintained and cultured on gelatin-coated tissue culture dishes in standard maintenance medium (Glasgow minimum essential medium with 10% fetal bovine serum and 1500 Units lif/ml (millipore), Glutamax, sodium pyruvate and non-essential amino acids [45]. For differentiation, ESCs were allowed to form embryoid bodies (EBs) in the IMDM/Ham-F12 (Cellgro) (3:1) supplemented with N2, B27, Penicillin/Streptomycin, 2mM GlutaMAX, 0.05% BSA, 5 ng/ml L-ascorbic acid (Sigma-aldrich), α-Monothioglycerol (MTG, Sigma-Aldrich). For mesoderm induction EBs were dissociated and reaggregated in the presence of Activin A, BMP4 and VEGF for 48 hours[46]. Cardiomyocytes were selected with Puromycin (2.5ug/ml) for 48h [44], dissociated and counted using an automated cell counter (Scepter 2.0, Millipore).

RNA suppression and cell cycle analysis

Cardiomyocytes were transfected with Lipofectamine RNAiMAX (Invitrogen). For *Alms1* knockdown experiments, *Alms1* ON-TARGETplus SMARTpool and *Alms1* siRNA (Ambion) or scrambled siRNA oligonucleotides (Dharmacon) and siRNA negative control (Ambion) were used at a final concentration of 100 nM for cell transfection. Forty-eight hours after transfection, cells were fixed and stained for flow cytometry with the following antibodies: anti-Ki67 (1:200, cat# ab15580, Abcam), -phospho-aurora A/B/C kinase (1:200, cat# 2914S, Cell Signaling), -phospho histone 3 (1:400, cat# ab5176, Abcam), -cardiac

troponin T (1:500, cat #13-11, Thermo scientific), -Thy1-APC (1:200, cat# 17-0902-81, eBioscience), with secondary detection using the appropriate Alexa Fluor-conjugated antibody (1:400, Invitrogen). For S-phase analysis, cardiomyocytes were treated with 100 μM EdU for 30 min prior to fixation and stained using Click-iT EdU cell proliferation kit (Invitrogen). For cell cycle analysis, dissociated cardiomyocytes were incubated for 30 min with 5 μM Vybrant Dye Cycle Ruby Stain (Invitrogen). For EdU analysis, cells were treated with 100 μM EdU for 30 minutes prior to isolation and fixation. EdU incorporation was detected using Click-it EdU Alexa Fluor Imaging Kit (Invitrogen) according to manufacturer's protocol. Cells were analysed on an Accuri C6 flow cytometer (BD Biosciences) using FlowJo software (Treestar).

Mice

The *Alms1*$^{Gt/Gt}$ mice (B6.129P2-*Alms1*$^{Gt(XH152)Byg}$/Pjn) used in this study were generated from gene-trapped ES cells (MMRC#008633)[26,47]. Mice were fed *ad libitum* a 4K54 diet (PMI Nutrition International, St. Louis, MO) and provided an unlimited access to water in a temperature/humidity controlled setting with a 12 hour light/dark cycle at The Jackson Laboratory Research Animal Facility. All mouse protocols used in this study were approved by the JAX institutional Animal Care and Use Committee. Mouse hearts were extracted from mice euthanized by carbon dioxide asphyxiation and allowed to contract in phosphate buffered saline for 5–10 minutes and immediately placed in 4% paraformaldeyde at 4 °C overnight. Subsequently, tissues were embedded in paraffin, sectioned, and immunostained as previously reported[48]. The aMHC promoter-driven EGFP-IRES-puromycin transgenic mice (alphaMHC-GFP), in which only cardiomyocytes express the green fluorescent protein (GFP) facilitate rapid and efficient isolation of cardiomyocytes[23]. Hearts from these mice were dissociated using collagense II/TrypLE. GFP+ cardiomyocytes were isolated by Fluorescence Activated Cell Sorting (FACS) using an SH800 sorter (Sony Biotechnology).

Histology and immunohistochemistry

Paraffin-embedded heart sections were rehydrated, followed by antigen retrieval. Immunostaining was performed on cultured cardiomyocytes and mouse cardiac tissue with primary antibodies against Ki67, cardiac troponin T, α-sarcomeric actinin, phosphohistone-H3, phosphoaurora A/B/C, or activated caspase-3 followed by secondary detection with appropriate Alexa Fluor conjugated antibodies. Additional staining was done with wheat germ agglutinin conjugated with Alexa Fluor-647 dye to show cell boundaries. Analyses using confocal microscopy were quantified in a blinded fashion by 2 independent observers. All images were acquired with a Zeiss LSM 510 Meta Confocal system and analyzed with Volocity imaging software. Puromycin selected cardiomyocytes were fixed in 4% formaldehyde. Cardiomyocytes were permabilized with 0.5% saponin/PBS and stained with antibodies against cTnT or isotype control antibodies followed the appropriate Alexa Fluor-conjugated antibody (Invitrogen).

Determination of cardiomyocyte density and size

Postnatal day 15 wild-type and *Alms1*$^{Gt/Gt}$ mouse hearts were fixed with methanol, paraffin embedded, sectioned, deparaffinized, rehydrated, and subjected to citrate-based heat-

mediated antigen retrieval. Slides were incubated with 5 μg/ml Alexa Fluor 647-conjugated wheat germ agglutinin (Invitrogen) overnight at 4 °C and mounted in Vectashield containing DAPI (Vector Labs, CA). Image acquisition was performed on an EVOS epifluorescence microscope (Life Technologies). Cardiomyocyte cross sectional area was measured using an automated algorithm with NIH Image J 1.47i software analyzing 300 – 600 cells from 3–4 areas per mouse heart.

Quantitative qRT-PCR

RNA was extracted with TRIzol (Invitrogen). Reverse transcriptase–quantitative PCR (qPCR) was performed using the Superscript III first-strand synthesis system (Invitrogen) followed by use of TaqMan probes on the ABI 7900HT (Applied Biosystems) according to the manufacturer's protocols. Optimized primers from TaqMan Gene Expression Array were used. Expression levels were normalized to Gapdh expression. All samples were run at least intriplicate. Real-time PCR data were normalized and standardized with SDS2.2 software.

Quantitative fluorescence

To measure nuclear DNA content, 20um thick histology sections of the proband's heart were stained with DAPI. Using a Zeiss LSM 510 Meta confocal microscope and Zen software for image acquisition, the nuclear DNA content of cardiac myocytes was assayed by measuring the total fluorescence from each selected nucleus with Volocity™ imaging software. Background fluorescence was excluded prior to image acquisition using Zen software. Nuclei in contact with the edges of the image stack or touching other nuclei were excluded. The total DAPI fluorescence signal associated with diploid status was designated 1 in non-proliferating cells (negative for PH3 staining). The DNA content of proliferating cardiomyocytes (positive for PH3 staining) was compared to non-proliferating cells and displayed as a ratio of the total quantitative fluorescence. A value of 2 would indicate cells that have a full duplication of nuclear DNA prior to karyokinesis.

Supplementary Material

Refer to Web version on PubMed Central for supplementary material.

Acknowledgments

We thank the families presented in this report for their participation. We thank Dr. Peter Rainer for assistance with analysis of myocyte sizes, Dr Kenneth Boheler for providing mouse embryonic stem cells with the *Ncx*-puromycin transgene, and Dr Deepak Srivastava for providing αMHC-GFP transgenic mice. We also thank Drs. Loren Field, Charles Steenbergen, and E. Rene Rodriguez for helpful advice and guidance. Supported by funding from the JHU Friends in Red, the Zegar Family Foundation, The Michel Mirowski Discovery Fund (DPJ), Mrs. Seena Lubcher (DPJ), R01HL111198 and 4R00HL09223 (NIH/NHLBI)(CK), Maryland Stem Cell Research Fund(CK), Magic That Matters Fund (CK), the Lundbeck Foundation (PA), and HD036878 (NIH) (JKN and GBC). The JHU Center for Inherited Disease Research is supported by funding from NIH contract HHSN268200782096C.

References

1. Drenckhahn JD, et al. Compensatory growth of healthy cardiac cells in the presence of diseased cells restores tissue homeostasis during heart development. Dev Cell. 2008; 15:521–33. [PubMed: 18854137]

2. Meilhac SM, et al. A retrospective clonal analysis of the myocardium reveals two phases of clonal growth in the developing mouse heart. Development. 2003; 130:3877–89. [PubMed: 12835402]
3. Pasumarthi KB, Field LJ. Cardiomyocyte cell cycle regulation. Circ Res. 2002; 90:1044–54. [PubMed: 12039793]
4. Soonpaa MH, Field LJ. Survey of studies examining mammalian cardiomyocyte DNA synthesis. Circ Res. 1998; 83:15–26. [PubMed: 9670914]
5. Mahmoud AI, et al. Meis1 regulates postnatal cardiomyocyte cell cycle arrest. Nature. 2013; 497:249–53. [PubMed: 23594737]
6. Chang KT, Taylor GP, Meschino WS, Kantor PF, Cutz E. Mitogenic cardiomyopathy: a lethal neonatal familial dilated cardiomyopathy characterized by myocyte hyperplasia and proliferation. Hum Pathol. 2010; 41:1002–8. [PubMed: 20303141]
7. Pasumarthi KB, Nakajima H, Nakajima HO, Soonpaa MH, Field LJ. Targeted expression of cyclin D2 results in cardiomyocyte DNA synthesis and infarct regression in transgenic mice. Circ Res. 2005; 96:110–8. [PubMed: 15576649]
8. Cottage CT, et al. Cardiac Progenitor Cell Cycling Stimulated by Pim-1 Kinase. Circ Res. 2010; 106:891–901. [PubMed: 20075333]
9. Wei Y, Mizzen CA, Cook RG, Gorovsky MA, Allis CD. Phosphorylation of histone H3 at serine 10 is correlated with chromosome condensation during mitosis and meiosis in Tetrahymena. Proc Natl Acad Sci U S A. 1998; 95:7480–4. [PubMed: 9636175]
10. Kim Y, Holland AJ, Lan W, Cleveland DW. Aurora kinases and protein phosphatase 1 mediate chromosome congression through regulation of CENP-E. Cell. 2010; 142:444–55. [PubMed: 20691903]
11. Yang KT, et al. Aurora-C Kinase Deficiency Causes Cytokinesis Failure in Meiosis I and Production of Large Polyploid Oocytes in Mice. Mol Biol Cell. 2010; 21:2371–2383. [PubMed: 20484572]
12. Seki A, Coppinger JA, Jang CY, Yates JR, Fang G. Bora and the kinase Aurora a cooperatively activate the kinase Plk1 and control mitotic entry. Science. 2008; 320:1655–8. [PubMed: 18566290]
13. Zimmerman RS, et al. A novel custom resequencing array for dilated cardiomyopathy. Genetics in Medicine. 2010; 12:268–278. [PubMed: 20474083]
14. Collin GB, et al. Mutations in ALMS1 cause obesity, type 2 diabetes and neurosensory degeneration in Alstrom syndrome. Nat Genet. 2002; 31:74–8. [PubMed: 11941369]
15. Marshall JD, et al. Spectrum of ALMS1 variants and evaluation of genotype-phenotype correlations in Alstrom syndrome. Hum Mutat. 2007; 28:1114–23. [PubMed: 17594715]
16. Alstrom CH, Hallgren B, Nilsson LB, Asander H. Retinal degeneration combined with obesity, diabetes mellitus and neurogenous deafness: a specific syndrome (not hitherto described) distinct from the Laurence-Moon-Bardet-Biedl syndrome: a clinical, endocrinological and genetic examination based on a large pedigree. Acta Psychiat Neurol Scand. 1959; 34:1–35.
17. Girard D, Petrovsky N. Alstrom syndrome: insights into the pathogenesis of metabolic disorders. Nat Rev Endocrinol. 2011; 7:77–88. [PubMed: 21135875]
18. Marshall JD, Maffei P, Collin GB, Naggert JK. Alstrom syndrome: genetics and clinical overview. Curr Genomics. 2011; 12:225–35. [PubMed: 22043170]
19. Bond J, et al. The importance of seeking ALMS1 mutations in infants with dilated cardiomyopathy. J Med Genet. 2005; 42:10.
20. Li F, Wang X, Capasso JM, Gerdes AM. Rapid transition of cardiac myocytes from hyperplasia to hypertrophy during postnatal development. J Mol Cell Cardiol. 1996; 28:1737–46. [PubMed: 8877783]
21. Soonpaa MH, Kim KK, Pajak L, Franklin M, Field LJ. Cardiomyocyte DNA synthesis and binucleation during murine development. Am J Physiol. 1996; 271:H2183–H2189. [PubMed: 8945939]
22. Ieda M, et al. Cardiac Fibroblasts Regulate Myocardial Proliferation through β Integrin Signaling. Developmental Cell. 2009; 16:233–244. [PubMed: 19217425]
23. Ieda M, et al. Direct reprogramming of fibroblasts into functional cardiomyocytes by defined factors. Cell. 2010; 142:375–86. [PubMed: 20691899]

24. Boheler KR, et al. Embryonic stem cell-derived cardiomyocyte heterogeneity and the isolation of immature and committed cells for cardiac remodeling and regeneration. Stem Cells Int. 2011; 2011:214203. [PubMed: 21912557]
25. Walsh S, Ponten A, Fleischmann BK, Jovinge S. Cardiomyocyte cell cycle control and growth estimation in vivo--an analysis based on cardiomyocyte nuclei. Cardiovasc Res. 2010; 86:365–73. [PubMed: 20071355]
26. Collin GB, et al. Alms1-disrupted mice recapitulate human Alstrom syndrome. Hum Mol Genet. 2005; 14:2323–33. [PubMed: 16000322]
27. Rash JE, Shay JW, Biesele JJ. Cilia in cardiac differentiation. J Ultrastruct Res. 1969; 29:470–84. [PubMed: 5365371]
28. Kim S, et al. Nde1-mediated inhibition of ciliogenesis affects cell cycle re-entry. Nat Cell Biol. 2011; 13:351–360. [PubMed: 21394081]
29. Li A, et al. Ciliary transition zone activation of phosphorylated Tctex-1 controls ciliary resorption, S-phase entry and fate of neural progenitors. Nat Cell Biol. 2011; 13:402–411. [PubMed: 21394082]
30. Ajima R, Hamada H. Wnt signalling escapes to cilia. Nat Cell Biol. 2011; 13:636–637. [PubMed: 21633348]
31. Kwon C, et al. Canonical Wnt signaling is a positive regulator of mammalian cardiac progenitors. Proc Natl Acad Sci U S A. 2007; 104:10894–9. [PubMed: 17576928]
32. Logan CY, Nusse R. The Wnt signaling pathway in development and disease. Annu Rev Cell Dev Biol. 2004; 20:781–810. [PubMed: 15473860]
33. Hayward P, Kalmar T, Arias AM. Wnt/Notch signalling and information processing during development. Development. 2008; 135:411–24. [PubMed: 18192283]
34. Knorz VJ, et al. Centriolar association of ALMS1 and likely centrosomal functions of the ALMS motif-containing proteins C10orf90 and KIAA1731. Mol Biol Cell. 2010; 21:3617–29. [PubMed: 20844083]
35. Hinchcliffe EH. Cell cycle: seeking permission from the mother centriole. Current Biology. 2003; 13:R646–648. [PubMed: 12932343]
36. Collin GB, et al. The Alström Syndrome Protein, ALMS1, Interacts with α-Actinin and Components of the Endosome Recycling Pathway. PLoS One. 2012; 7:e37925. [PubMed: 22693585]
37. Fielding AB, Willox AK, Okeke E, Royle SJ. Clathrin-mediated endocytosis is inhibited during mitosis. Proc Natl Acad Sci U S A. 2012; 109:6572–7. [PubMed: 22493256]
38. Fielding AB, Royle SJ. Mitotic inhibition of clathrin-mediated endocytosis. Cell Mol Life Sci. 2013; 70:3423–33. [PubMed: 23307073]
39. Sager PR, Brown PA, Berlin RD. Analysis of transferrin recycling in mitotic and interphase HeLa cells by quantitative fluorescence microscopy. Cell. 1984; 39:275–82. [PubMed: 6498936]
40. Li H, Durbin R. Fast and accurate long-read alignment with Burrows–Wheeler transform. Bioinformatics. 2010; 26:589–595. [PubMed: 20080505]
41. Li H, et al. The Sequence Alignment/Map format and SAMtools. Bioinformatics. 2009; 25:2078–2079. [PubMed: 19505943]
42. Ng SB, et al. Targeted capture and massively parallel sequencing of 12 human exomes. Nature. 2009; 461:272–6. [PubMed: 19684571]
43. Simpson P, Savion S. Differentiation of rat myocytes in single cell cultures with and without proliferating nonmyocardial cells. Cross-striations, ultrastructure, and chronotropic response to isoproterenol. Circulation Research. 1982; 50:101–116. [PubMed: 7053872]
44. Yamanaka S, Zahanich I, Wersto RP, Boheler KR. Enhanced Proliferation of Monolayer Cultures of Embryonic Stem (ES) Cell-Derived Cardiomyocytes Following Acute Loss of Retinoblastoma. PLoS One. 2008; 3:e3896. [PubMed: 19066628]
45. Kwon C, et al. Notch post-translationally regulates beta-catenin protein in stem and progenitor cells. Nat Cell Biol. 2011; 13:1244–51. [PubMed: 21841793]

46. Kattman SJ, et al. Stage-specific optimization of activin/nodal and BMP signaling promotes cardiac differentiation of mouse and human pluripotent stem cell lines. Cell Stem Cell. 2011; 8:228–40. [PubMed: 21295278]

47. Jagger D, et al. Alstrom Syndrome protein ALMS1 localizes to basal bodies of cochlear hair cells and regulates cilium-dependent planar cell polarity. Hum Mol Genet. 2011; 20:466–81. [PubMed: 21071598]

48. Shenje LT, et al. Lineage tracing of cardiac explant derived cells. PLoS One. 2008; 3:e1929. [PubMed: 18414652]

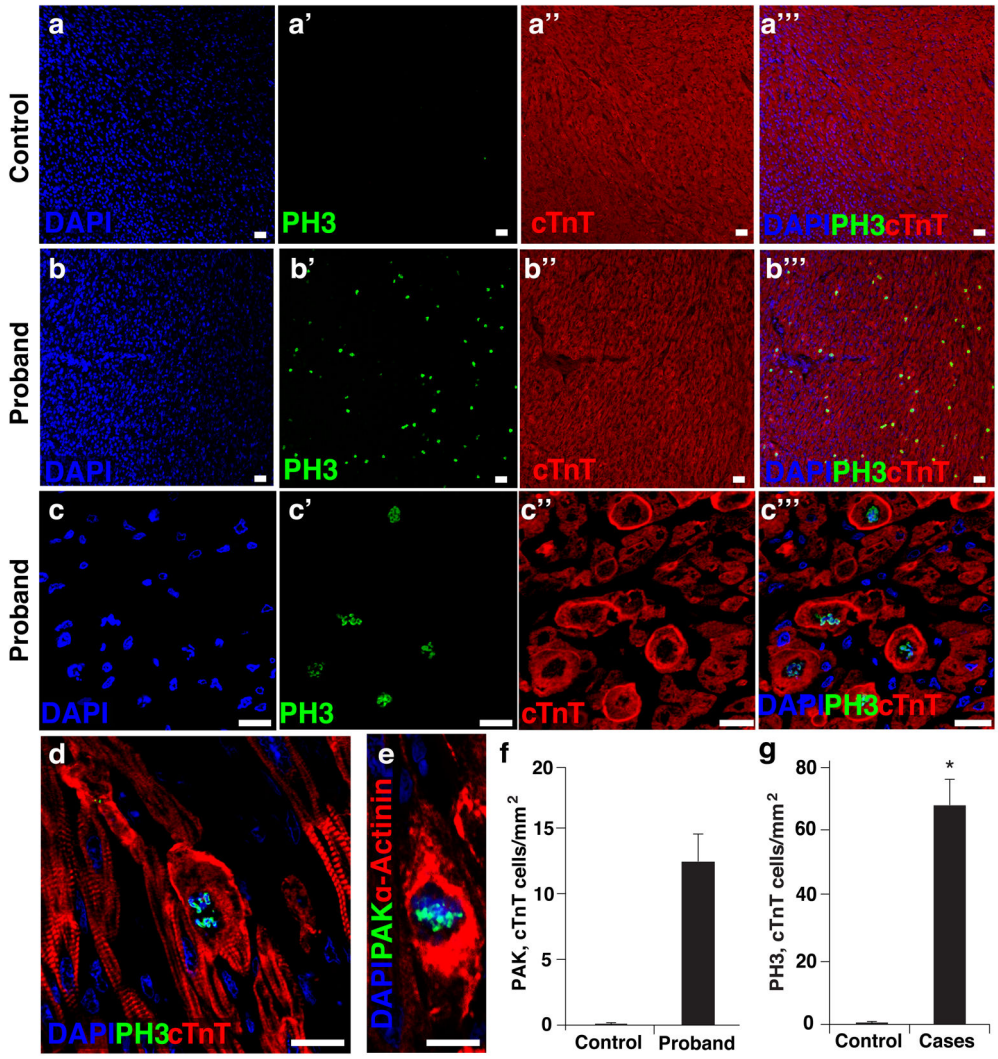

Figure 1. Increased cardiomyocyte proliferation in people with *ALMS1* mutations

(**a, b**) Representative confocal images of the proband heart vs. age-matched control; PH3 (green), troponin T (red), DAPI (blue). (**c**) Higher magnification confocal images of PH3-positive cardiomyocytes in the proband; PH3 (green), troponin T (red), DAPI (blue). (**d**.) Additional high-magnification confocal image of a PH3-positive cardiomyocyte in the proband; PH3 (green), troponin T (red), DAPI (blue). (**e**.) Phospho-aurora kinase (PAK) staining (green) is present in a dividing cardiomyocyte nucleus in the proband; PAK (green), α-sarcomeric actinin (red), DAPI (blue (**f**) The number of PAK-positive cardiomyocytes in the heart of the proband was compared to three age-matched controls with failing ventricles. (**g**) The number of PH3-positive cardiomyocytes in affected individuals was compared to three age-matched controls with failing ventricles. Error bars represent standard error of mean (SEM). All scale bars represent 10μm.

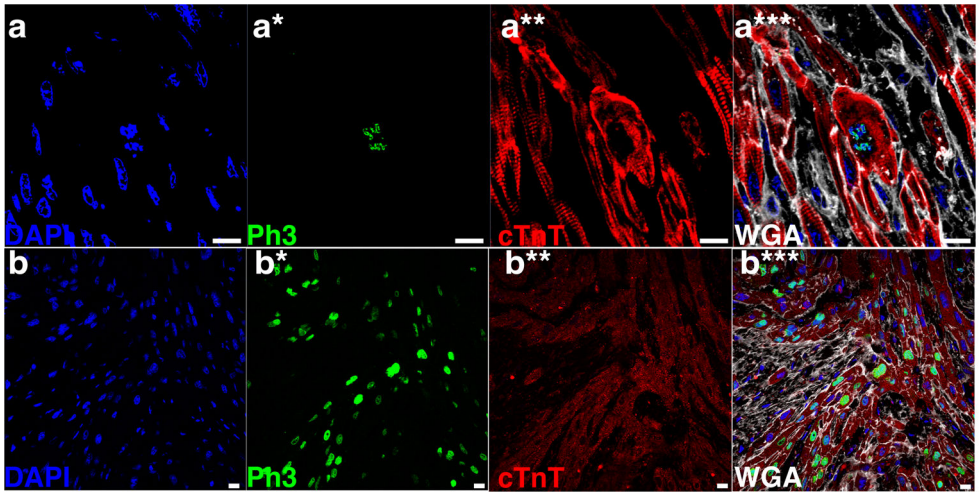

Figure 2. PH3-positive cardiomyocytes in the proband and another affected individual

Additional representative confocal microscopic images from the heart of the proband (a) and another individual with mitogenic cardiomyopathy (b) have high levels of phosphohistone-H3 (Ph3)-positivity. Images were obtained with confocal microscopy using immunostaining for Ph3 (green), α-sarcomeric actinin or troponin T (red), wheat germ agglutinin (white) to outline cell boundaries, and DAPI (blue) to highlight nuclei. Panels a and b – DAPI; panels a* and b* – Ph3; panels a** and b** – cTnT; panels a*** and b*** – merged images with DAPI, Ph3, cTnT, and WGA. Scale bars all indicate 10 μM.

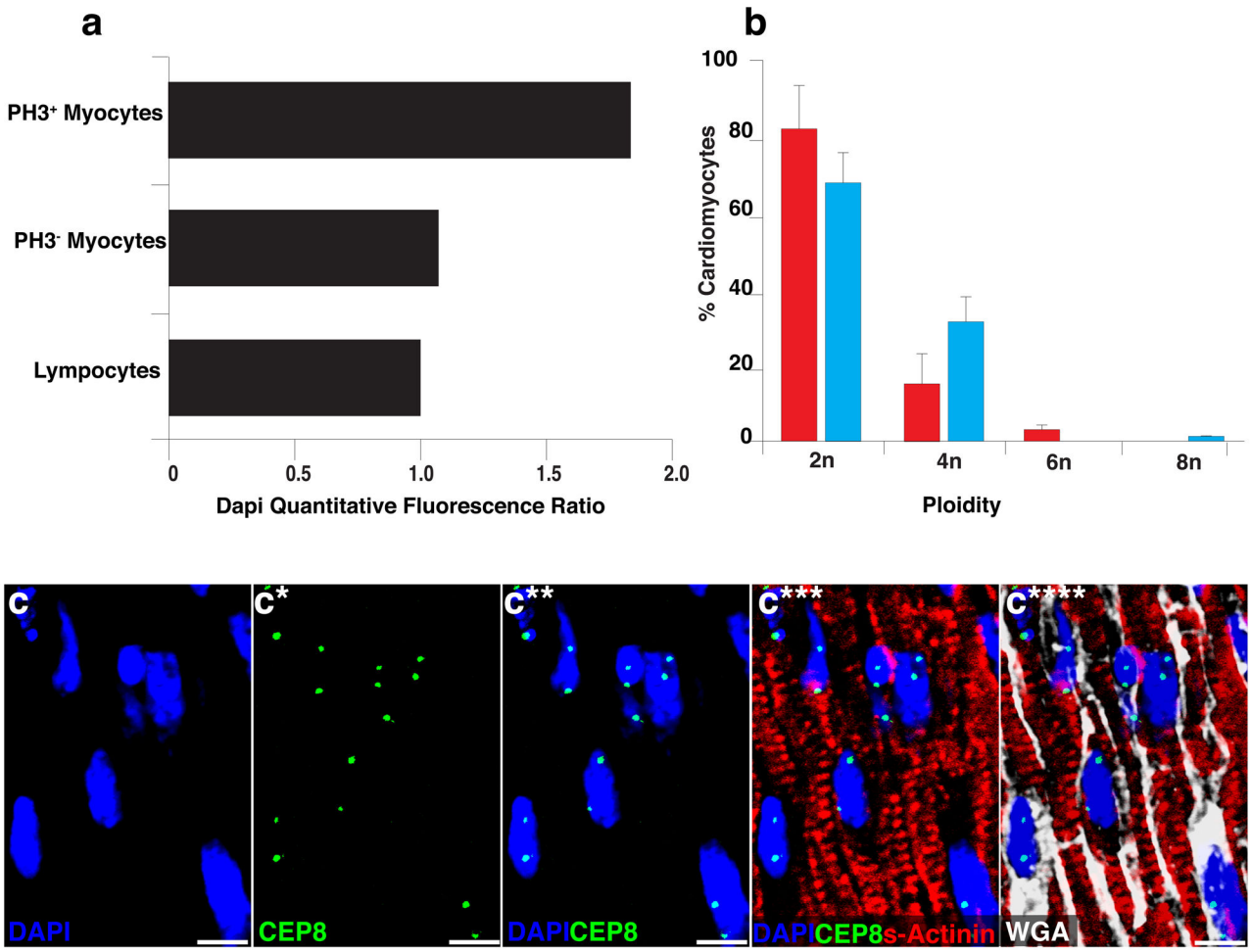

Figure 3. Human cells analyzed for ploidy status

(a.) The DNA content in dividing cardiomyocyte nuclei was compared to non-dividing nuclei (both cardiomyocytes and non-cardiomyocytes) in the proband using quantitative confocal laser cytometry with DAPI nuclear staining. The ratio of DNA in nuclei from proliferating cardiomyocytes compared to non-proliferating (cardiomyocyte and lymphocyte) nuclei in the proband is 1.9, indicating predominantly 4N chromosomal content in these cells. (b.) Summary of the ploidy analysis using centromeric probes for 4 affected individuals and 2 unaffected controls. Error bars indicate S.E.M.. (c.) An example of ploidy analysis using one of the centromere FISH probes for chromosome 8 (CEP8) in an affected individual. Color staining is shown in the bottom left. Scale bars indicate 10 μM; These five panels are the same field with: C) DAPI; C*) CEP8; C**) DAPI and CEP8; C***) DAPI, CEP8 and sarcomeric actinin; and C****) DAPI, CEP8, sarcomeric actinin, and WGA.

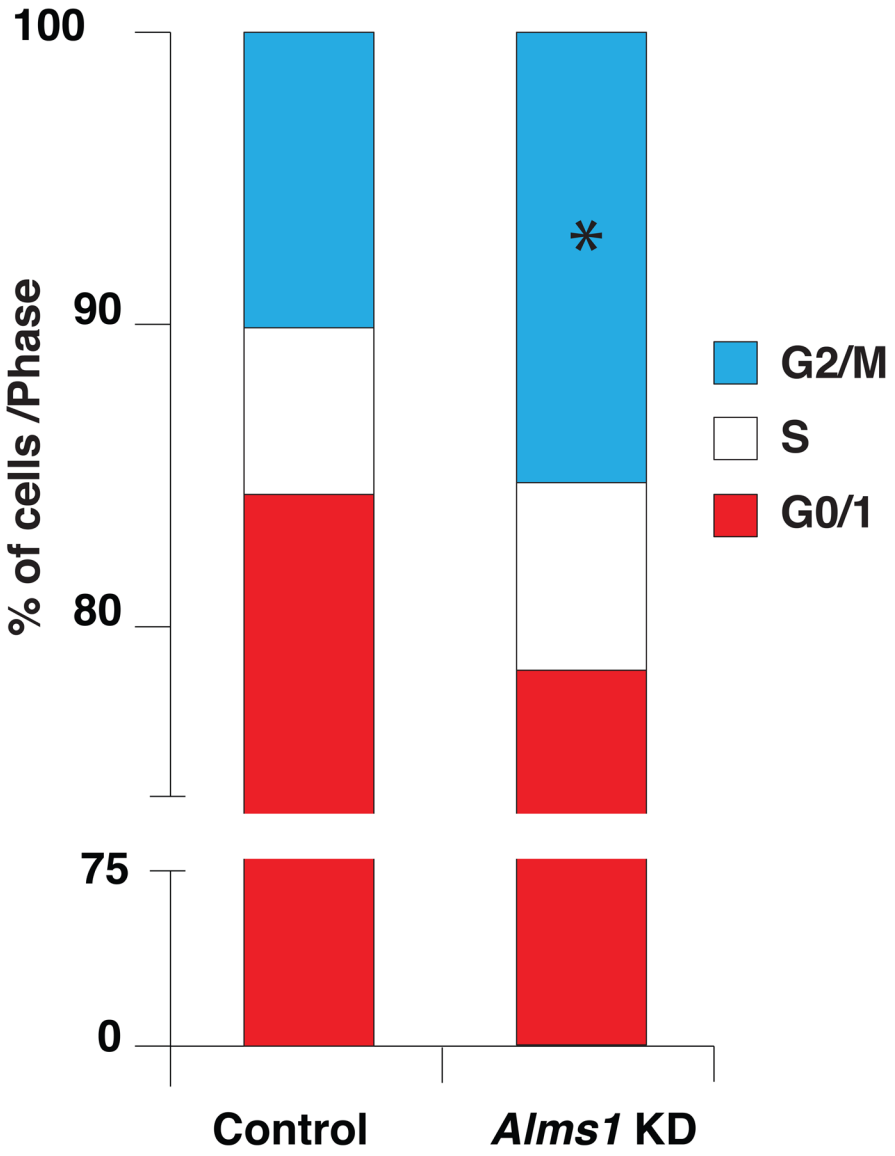

Figure 4. Knockdown of *Alms1* increases the number of cells in G2/M phases in cardiomyocyte enriched cultures

Comparison of the % of cells in different phases of cell cycle between control transfection and *Alms1* knockdown (KD) using siRNA; red = G0 or G1 phase, white = S phase, blue = G2 or M phase. (*) refers to P< 0.05 using unpaired Student's *t*-test.

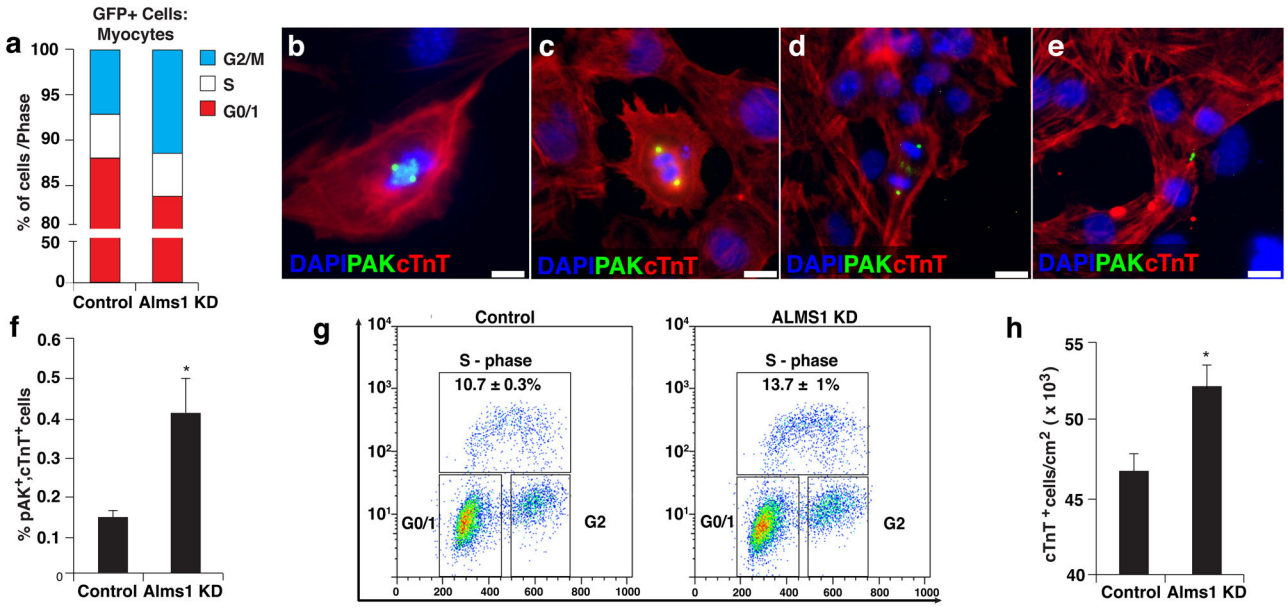

Figure 5. Increased cardiomyocyte proliferation in cultured cells after *Alms1* knockdown

(**a**.) Comparison of α-MHC-GFP positive cardiomyocytes in different phases of cell cycle after control siRNA transfection compared with *Alms1* knockdown (KD) by siRNA; red = G0 or G1 phase, white = S phase, blue = G2 or M phase; N=3. *Alms1* KD increases the proportion of cells in G2/M phase (blue). (**b., c., d., e**.) PAK-positive cardiomyocytes in different phases of mitosis; cTnT (red), PAK (green), and DAPI (blue); b is prophase, c is metaphase, d is anaphase, e is telophase. (**f**.) Flow cytometry of puromycin-selected cardiomyocytes ($cTnT^+$ cells) shows that after *Alms1* knockdown (KD), there is increased PAK expression compared to controls; N=3. (**g**.) Scatter plot showing increased incorporation of EdU (Y-axis) and increased DNA content by DAPI (X-axis) in puromycin-selected ($cTnT^+$) cardiomyocytes with *ALMS1* KD; N=15. (**h**.) Total number of puromycin-selected cardiomyocytes after *Alms1* knockdown (KD) is increased compared to controls; N=4. In all Figures, (*) refers to $P<0.05$ using Student's *t*-test. Error bars represent standard error of mean (SEM), and all scale bars represent 5 μM.

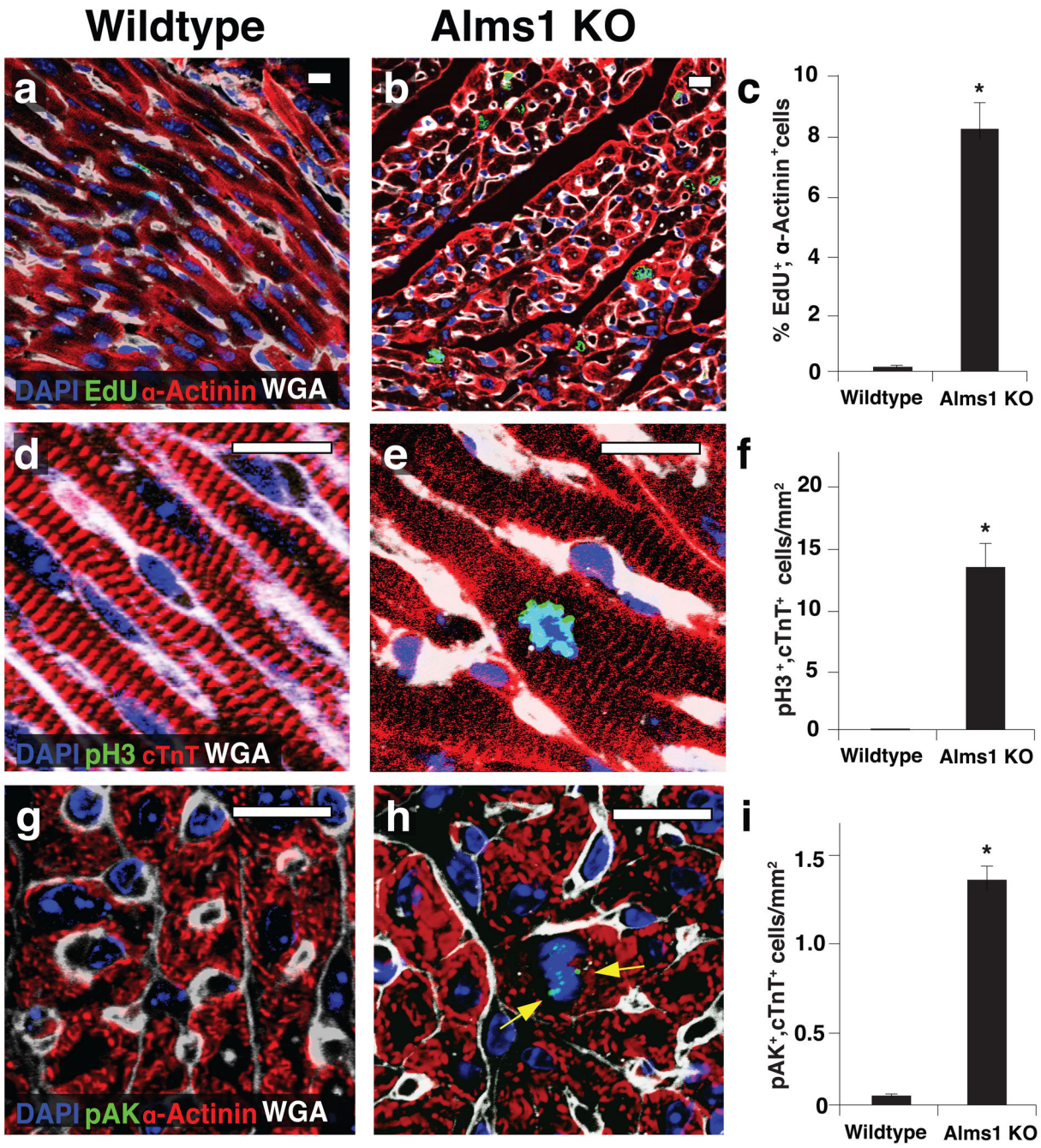

Figure 6. Increased cardiomyocyte proliferation in homozygous *Alms1*$^{Gt/Gt}$ mutant mice

(**a, b**.) Representative confocal images demonstrating EdU (green) incorporation in *Alms1*$^{Gt/Gt}$ vs. wild-type littermate control mouse cardiac myocytes; α-sarcomeric actinin (red), wheat germ agglutinin (WGA; white), and DAPI (blue). (**c**.) Bar graph comparing cardiomyocyte EdU incorporation in *Alms1*$^{Gt/Gt}$ mutant (KO) vs. wild-type littermate control mice (N=4 each). (**d, e**.) Representative confocal images demonstrating PH3 (green) in a cardiomyocyte nucleus in a *Alms1*$^{Gt/Gt}$ mutant vs. wild-type littermate control mouse, with cTnT (red), wheat germ agglutinin (white), and DAPI (blue). (**f**.) Comparison of the

number of PH3-positive cardiomyocytes in *Alms1*$^{Gt/Gt}$ (KO) vs. wild-type littermate control mice (N=3 each). (**g, h**.) Representative confocal images demonstrating PAK staining (green) is present in a dividing cardiomyocyte nucleus in an *Alms1*$^{Gt/Gt}$ mouse (KO); DAPI (blue) highlights the nucleus, which is surrounded by α-sarcomeric actinin (red) to highlight cardiomyocytes and WGA (white) to identify cell boundaries. (**i**.) Comparison of the number of PAK-positive cardiomyocytes in *Alms1*$^{Gt/Gt}$ (KO) vs. wild-type controls. All scale bars represent 10μm. Error bars represent S.E.M.. N=3 each.

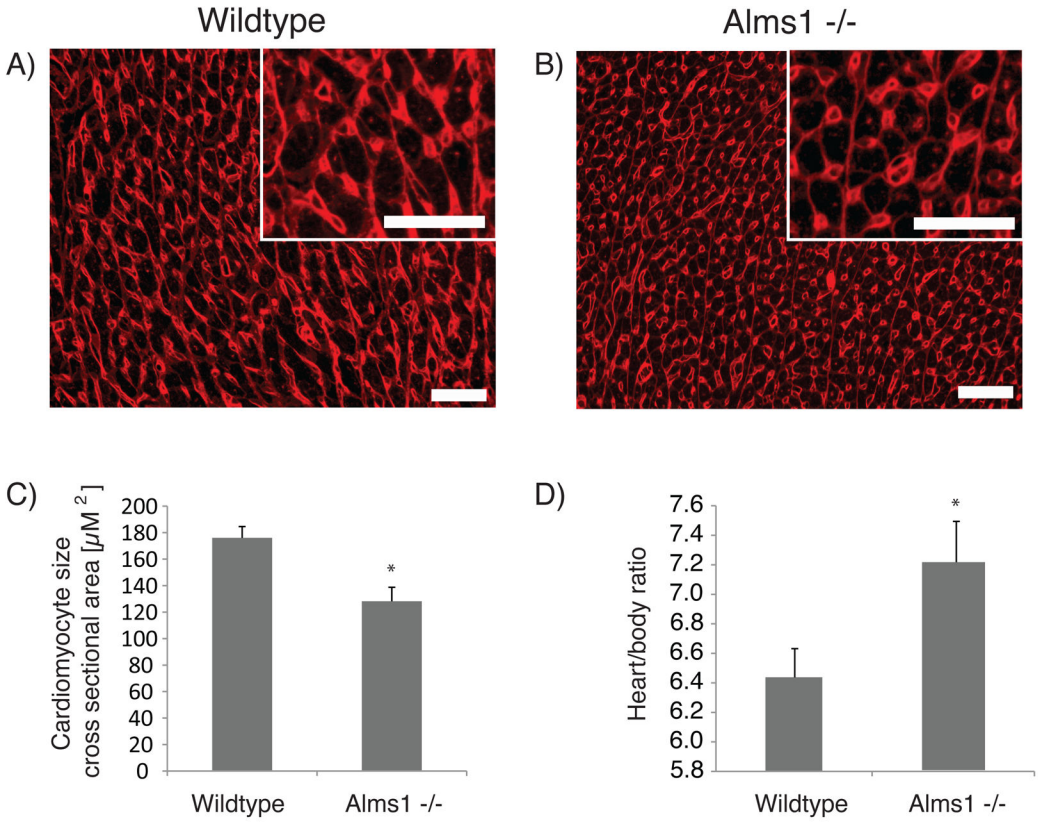

Figure 7. Increased cardiomyocyte density and normalized heart size in homozygous *Alms1*$^{Gt/Gt}$ mutant mice

Representative images of (A.) wild-type and (B.) *Alms1*$^{Gt/Gt}$ hearts stained with wheat germ agglutinin (white) and cTnT (red); scale bars = 50 uM. (C) Measured cardiomyocyte cross sectional area, N=12 each. (D) Heart/body weight ratios, N=16 for WT and N=7 for *Alms1*−/−; error bars represent S.E.M., (*) indicates P<0.05 using Student's *t*-test.

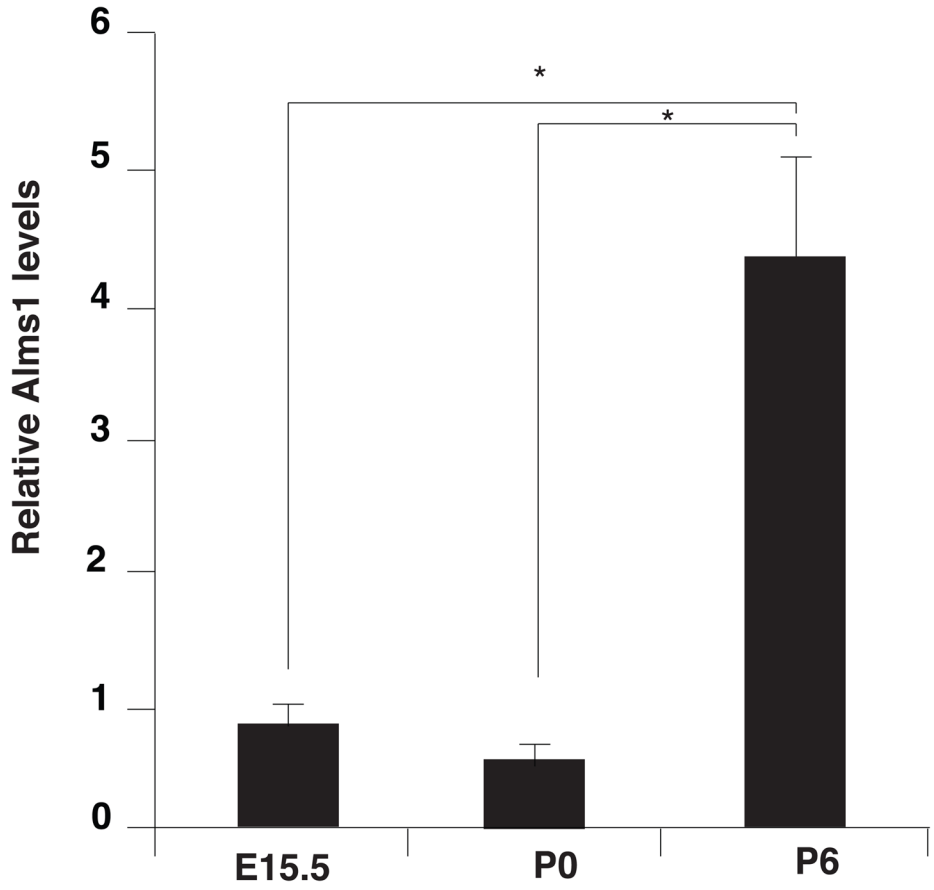

Figure 8. Perinatal expression of *Alms1* in murine cardiomyocytes

Murine GFP-positive cardiomyocytes were isolated from α-MHC-GFP transgenic mice by FACS. *Alms1* mRNA levels were normalized to *Gapdh*. Relative *Alms1* mRNA levels at embryonic day 15.5 (ED15.5; N=4) and postnatal day 0 (P0; N=4) were compared by student's T-Test to postnatal days 5.5/6.5 (P5/6; N=10), p=0.02 and p=0.013, respectively. (*) denotes P<0.05. There was no significant difference in *Alms1* expression between days E15.5 and P0; error bars indicate S.E.M.

Table 1

Filtered Exome Sequencing Results

Gene	Variant cDNA	Variant protein	Transcript Accession number	Allele frequency in 1000 Genomes Nov 2010	Present in Affected Sibling
ALMS1	c.1794_1801dup8	p.Lys601Arg_fsX3	NM_015120	-	Yes
	c.11116_11134del19	p.Arg3706Leu_fsX11	NM_015120	-	Yes
CD248	c.683C>G	p.Pro228Leu	NM_020404	-	No
	c.1235C>G	p.Pro412Arg	NM_020404	-	No
FERMT1	c.292C>T	p.Arg98Cys	NM_017671	-	Yes
	c.1555G>T	p.Val519Leu	NM_017671	-	Yes
FRMD4B	c.1424C>T	p.Pro475Leu	NM_015123	0.6	Not tested
	c.2309A>C	p.Asn770Thr	NM_015123	-	Yes
RGS3	c.231G>T	p.Gln77His	NM_144489	1.2	Not tested
	c.1327G>T	p.Ala443Ser	NM_021106	0.1	Not tested
RYR3	c.4529T>C	p.Val1510Ala	NM_001036	-	Yes
	c.14128G>A	p.Asp4710Asn	NM_001036	-	No
SNX19	c.842C>T	p.Ala281Val	NM_014758	0.5	Not tested
	c.2683C>T	p.Arg895Trp	NM_014758	-	No

Genes in which two rare variants are present in the proband, inherited in a recessive manner from each parent. Variants present in the 1000 Genomes dataset by 11/2010 were prioritized lower. Those in which one or both variants was not present in the affected sibling were excluded.

Table 2

Mutations in *ALMS1* in people with mitogenic cardiomyopathy:

Individual	Exon	cDNA	protein
1a	8	1794_1801dup8	Lys601Arg_fsX3
	16	11116_11134del19	Arg3706Leu_fsX11
1b	8	1794_1801dup8	Lys601Arg_fsX3
	16	11116_11134del19	Arg3706Leu_fsX11
2a	8	4296_4299delCACA	His1432Gln_fsX40
	8	5926delG	Glu1976Ser_fsX8
2b	8	4296_4299delCACA	His1432Gln_fsX40
	8	5926delG	Glu1976Ser_fsX8
3a	8	1894C>T	Gln632Ter
	8	1894C>T	Gln632Ter
3b	8	1894C>T	Gln632Ter
	8	1894C>T	Gln632Ter

The proband and her sibling are 1a and 1b. Individuals 2a, 2b, 3a, and 3b are affected sibling pairs that were previously reported with this phenotype. Parental testing in 2a and 2b demonstrated compound heterozygosity, because both parents are heterozygous for a single *ALMS1* mutation.